Mu, N., Fu, Y., Schulz, H.-M., van Berk, W. (2016): Authigenic albite formation due to water-rock interactions - Case study: Magnus oilfield (UK, Northern North Sea). - *Sedimentary Geology*, *331*, p. 30-41.

DOI: http://doi.org/10.1016/j.sedgeo.2015.11.002

Authigenic albite formation due to water-rock interactions - Case study: Magnus oilfield (UK, Northern North Sea)

Nana Mu[1], Yunjiao Fu[2], Hans-Martin Schulz[1,*], and Wolfgang van Berk[2]

[1]Helmholtz Centre Potsdam–GFZ German Research Centre for Geosciences, Section 4.3 Organic Geochemistry, Telegrafenberg, D-14473 Potsdam, Germany

[2]Clausthal University of Technology, Department of Hydrogeology, Leibnizstraße 10, D-38678 Clausthal-Zellerfeld, Germany

*Corresponding author: Tel.: +49 331 288-1789; Fax: +49 331 288-1782; Email address: schulzhm@gfz-potsdam.de

Abstract

It is the aim of this contribution to test whether organic-inorganic interactions could induce the formation of authigenic albite. This concept and related results are being compared with modelling scenarios which are purely based on inorganic geochemical reactions. In order to unravel the pathway of authigenic albite formation, this paper presents results of a multidisciplinary study from imaging, geochemistry, mineralogy, and hydrogeochemical modelling. The Jurassic reservoir sandstones of the Magnus oilfield (UK, North Sea) were chosen as a test site.

Albite occurs with 4-18 wt. % in the Magnus sandstones and its contents vary with depth. However, albite contents increase with increasing K-feldspar contents and decreasing grain size. It occurs in three forms: (1) as lamellae in perthite, (2) as overgrowth on/in corroded feldspar, and, (3) as cloudy replacing albite patches in K-feldspar. The albite overgrowth has the highest chemical purity (100% albite) while albite lamellae and replacing albite patches are slightly less pure (containing 1-4% anorthite). Albite appears non-altered, and has an euhedral morphology and dull cathodoluminescence. It commonly co-occurs with corroded K-feldspar grains.

The precipitation of diagenetic albite in the Magnus sandstones is attributed to deep burial 80 Ma ago and may have continued until today at temperatures between 90-120°C. The results of hydrogeochemical modelling offer two possible pathways for the authigenic albite formation: (1) Dissolution of unstable minerals (such as kaolinite and chalcedony) coupled to reduction of ferric iron minerals by products generated during oil generation, migration and degradation; (2) Dissolution of non-end member feldspar, such as K-feldspar with 10% albite, coupled to illite formation can account for trace amounts of albite due to an elevated Na^+/K^+ activity ratio in the pore water.

Keywords: Albite; Jurassic; sandstone; rock-water interaction; Magnus oilfield; North Sea

1. Introduction and aim

In hydrocarbon-bearing systems, the driving force of organic-inorganic interactions is the conversion of thermodynamically labile organic compounds into reactive and soluble inorganic components. Water is the matrix for such complex and interrelated hydrogeochemical reactions. However, such processes are also dependent on a variety of other controls such as temperature and/or pressure. The composition of the mineral phase assemblage, the type of water (e.g., the content of total dissolved solids, pH, E_H, etc.) and of co-existing gases (e.g., CO_2 partial pressure) are further important controls.

In oilfields the hydrolytic disproportionation of low-molecular hydrocarbons across the reactive oil-water transitional zone may stimulate organic-inorganic interactions. It is argued to be result of an irreversible production of carbonic acid. This basic assumption led Helgeson et al. (1993) in their ground-breaking article to speculate about metastable equilibria between petroleum, oilfield waters, and authigenic mineral assemblages. One topic in this respect was whether organic-inorganic interactions could lead to albite formation. In this contribution we test whether such a hypothesis is valid for albitization of feldspar or precipitation of albite crystals, and will compare the measured/observed results with results from alternative modelling concepts which are exclusively based on inorganic geochemical reactions triggered by temperature and pressure.

In a first step, we present results about the content, petrographic characteristics and chemical composition of albite in the Jurassic sandstone reservoir of the Magnus oilfield leading to first considerations about the origin and potential hydrogeochemicalconditions of albite formation. In

a second step, results of hydrogeochemical models calculated by using the computer code Phreeqc are presented. The results of these conceptual model approaches aim to unravel possible pathways of authigenic albite formation in a quantitative way regarding to thermodynamic principles. Baseline data for modelling are mineral assemblages, data about formation water composition, potential slight oil degradation and burial history.

2. A brief review about physicochemical controls of albite formation or albitization

Authigenic albite commonly occurs in many kinds of sedimentary rocks (Kastner, 1971; Kastner and Siever, 1979), and its formation and occurrence in sandstones is widely known in numerous sedimentary basins worldwide (Walker, 1984; Gold, 1987; Saigal et al., 1988; Pittman, 1988; Milliken, 1989; Aagaard et al., 1990; Morad et al., 1990; González-Acebrón et al., 2010). Formation of authigenic albite in sandstones is reported to be coupled to high temperatures between 100-150° C (Milliken et al, 1981; Boles, 1982; Surdam et al., 1989), but it also occurs at lower temperatures in the range of 60-100° C (Saigal et al., 1988; Morad et al., 1990; Aagaard et al., 1990). However, albite formation increases with depth (Saigal et al., 1988; Aagaard et al., 1989; Milliken, 1989; Morad et al., 1990), and its precipitation at depth is reflected by distinctive textures such as the "chessboard" texture (Walker, 1984), blocky to tabular sector extinction patterns (Gold, 1987), or by albite overgrowths on plagioclase grains (Milliken, 1989). The growth of authigenic albite in sandstones is related to two processes: formation of overgrowth due to precipitation from saturated solutions, or replacement of K-feldspar or plagioclase by albite (Hirt et al., 1993; Bozau et al., 2015). The main cause of albite formation may be coupled to illite formation (Aagaard et al., 1990; Bjorlykke et al., 1995). Since the rate of illite formation increases at temperatures close to 100° C, precipitation of illite at the expense of smectite and

kaolinite removes potassium from the pore water resulting in relatively high Na/K ratios (Aagaard et al., 1990; Bjorlykke et al., 1995). In such case the pore water becomes saturated/oversaturated with respect to albite and undersaturated with respect to K-feldspar, enabling albite formation (Aagaard et al., 1990; Bjorlykke et al., 1995). During this process, the original mineral composition can be significantly altered, whilst several diagenetic products such as calcite, kaolinite, dickite and illite can be formed modifying the pore size and geometry (Boles, 1982; Saigal et al., 1988; Morad et al., 1990).

3. Geological background of the Magnus oilfield

The Magnus oilfield is located within UKCS block 211/12a and 211/7a in the North Viking Graben of the Northern North Sea (Fig. 1A). It situates in a south-eastward dipping, tilted fault-block structure. The areal extent of the field is defined to the east by the oil-water contact (3,150 m subsea), and to the west by a depositional pinch-out to the north and south, and by a sub-Cretaceous unconformity in the central crestal region (Fig. 1A, Macaulay et al., 1992). The main reservoir unit of the Magnus field is the Upper Jurassic Magnus Sandstone Member (MSM) which is intercalated within the carbonaceous Kimmeridge Clay Formation (Fig. 1B). The MSM was deposited in the middle-fan setting of a submarine fan (De'Ath and Schuyleman, 1981; Shepherd, 1991; Macaulay et al., 1992). Oil in the Magnus sandstones was sourced from both the overlying and underlying Kimmeridge Clay Formation (De'Ath and Schuyleman, 1981; Barclay and Worden, 1998). The main source area lies to the east of the field although some oil was probably also sourced from the north (Shepherd, 1991). The main phase of oil generation is thought to have commenced approximately 75 Ma BP (Maastrichtian-Campanian) (Shepherd, 1991), and migration probably took place during the early Tertiary (De'Ath and Schuyleman,

1981).

The Magnus sandstones comprise light grey, fine to medium-grained, poorly sorted sub-arkosic to arkosic sandstones, and are dominated by detrital quartz, K-feldspar, plagioclase, and minor mica (Fig.1; De'Ath and Schuyleman, 1981; Baines and Worden, 2004). Macaulay et al. (1993b) pointed out that the burial history of the Magnus sandstones can be divided into two stages: (1) structural uplift and tilting between 160 and 90 Ma, and (2) a continuous burial with an increase in temperature and pressure conditions after the Upper Cretaceous (ca. 90 Ma). Following the deposition of the Magnus sandstones, the sediments were shallowly buried during the late Jurassic followed by a depositional hiatus during the early Cretaceous as the reservoir was faulted and uplifted, thus exposed and eroded. A second break in deposition occurred in the mid-Cretaceous with a new uplifting of the Lower Cretaceous and Jurassic sediments. During these two uplift periods, the Magnus sandstones were exposed to subaerial erosion including a potential long-term infiltration of groundwater which led to feldspar dissolution and kaolinite precipitation. Since mid-Cretaceous, the Magnus sandstones rapidly subsided during the Tertiary and Quaternary. The main diagenetic events are thought to have occurred during this deep burial process and coincided with oil emplacement, including K-feldspar dissolution, quartz overgrowth, ankerite cementation, and formation of siderite, kaolinite and illite (Tab. 1; Fig. 2; Saigal et al., 1988; Emery et al., 1990, 1993; Macaulay et al., 1992, 1993a, 1993b; Barclay and Worden, 1998, 2000; Barclay et al., 2000; Worden and Barclay, 2000, 2003).

Numerous investigations have focussed on these main diagenetic processes of Jurassic sandstones in the Magnus oilfield (Emery et al., 1990, 1993; Macaulay et al., 1992, 1993a, 1993b; Barclay and Worden, 1998, 2000; Barclay et al., 2000; Worden and Barclay, 2000, 2003). However, authigenic albite and its potential formation pathways have not yet been studied

in detail. Furthermore, hydrogeochemical modelling results presented by Barclay and Worden (2000) did not include any result about albite. Their study was carried out to test whether quartz and other minerals observed in the Magnus sandstones can be formed as new diagenetic phases due to the reaction between K-feldspar and source rock-derived CO_2. However, albite may make up to 18 wt.-% of the bulk reservoir rock in the Magnus oilfield (measured by XRD; this study) either as a primary or secondary mineral.

4. Methodology

This study is based on the investigation of 24 core samples collected from well 211/12a-9 (Fig. 1A) from the oil leg down to the underlying water leg crossing the present oil-water transition zone. Prior to further preparations, all core samples were extracted for 24 hours using 99 n-hexane: 1 dichloromethane in a Dionex ASE 200 soxhlet at 50°C in order to remove freely accessible hydrocarbons. Selected samples were impregnated with blue epoxy prior to preparation of polished thin sections and later were studied with an optical microscope. Six representative thin sections were coated with carbon for further investigations of textures, authigenic minerals and their paragenetic relationships by using a Philips SEM-515 with an Edax PV 9100 energy-dispersive X-ray spectroscopy (EDS). Images under both scanning (SE) and backscattered scanning electron (BSE) modes were obtained. Energy-dispersive X-ray spectroscopy (EDS) analysis was conducted to study the chemical composition of feldspars. To study the cathodoluminescence of different feldspars, four thin sections were investigated by using a cold cathode luminescence device CITL 8200 MK3 coupled to a ZEISS "Amplival" microscope. Electron gun voltages and beam currents of 10 kV and 0.4 mA were used whilst the polished thin sections were held under vacuum between 0.07 and 0.01 Torr. In addition, freshly

broken rock chips were investigated by SEM to study mineral morphologies and dissolution/precipitation patterns. To determine and semi-quantify mineral assemblages, all core samples were grounded to powder for X-ray diffraction analysis (XRD) by using a BRUKER-axs D5000. X-ray fluorescence analyses (XRF) were also carried out on bulk samples by using PHILIPS PW2400 to analyse the element composition of whole rock in order to identify whether albite is the exclusive sodium-bearing mineral (comparison with XRD data). The grain size distribution was obtained by measuring the long axis of detrital grains and 100 grains per thin section were studied. The presented grain size values are the mean diameter of 100 grains.

Based on petrographic study of the Magnus sandstones, hydrogeochemical modelling was carried out using the computer code PHREEQC Interactive version 3.2 (Parkhurst and Appelo, 2013) to simulate a closed, isothermal and isochemical system in which a state of chemical equilibrium among the mineral assemblage, pore water and gas can be achieved based on chemical thermodynamics and mass balancing. This model does not take kinetic aspects into account. Therefore, modelling based on the thermodynamics of chemical equilibrium can be used to decipher reaction pathways because it illustrates how water-rock reactions in systems will evolve for equilibration (given sufficient time).

5. Results of microscopic, geochemical and mineralogical studies

The Magnus sandstones vary in grain size, sorting and mineralogical composition, and consist of 40-76 wt. % quartz (including detrital quartz and quartz cement), 16-33 wt. % feldspar (K-feldspar and plagioclase) and 0-5 wt. % muscovite. Minor accessories include pyrite, siderite, and ankerite. Most of the K-feldspar and oligoclase lack indications of alteration (Figs. 2A, 2H). However, some K-feldspar grains appear strongly corroded and altered (Figs. 2A, 2C-2E, and 5).

Albite is another main component in the Magnus sandstones.

5.1 Bulk mineralogy and geochemistry

Both the Na_2O and the albite content of the Magnus sandstones vary with depth (Fig. 3), and show a linear relationship (Fig. 4A). This fit may indicate that Na in the Magnus sandstones is mainly incorporated in albite which could be either in the form of albite grains or even albite lamellae in perthite. The K_2O and the K-feldspar content also vary greatly with depths. However, the K_2O values above the line of stoichiometric K-feldspar indicate the presence of other K-bearing minerals (mica, illite; Fig. 4B). In general, there are linear relationships between the Na_2O vs. the K_2O content, and between the albite and the K-feldspar content (Figs. 4C, 4D). Importantly, more albite occurs in samples which have higher feldspar contents (Fig. 4D). It is also noteworthy that the Na_2O and the albite contents show a relation with the grain size (Figs. 4E, 4F): a smaller grain size, higher Na_2O and albite contents.

5.2 Microscopy

Albite in the Magnus sandstones occurs in three forms (Table 2): (1) as regular/irregular lamellae in perthite (to a minor degree), (2) mostly as overgrowth/euhedral crystals on/in corroded feldspar (Figs. 2C, 2E, 2D, 5A and 5B), and (3) as irregular patches in albitized grains or even as albite pseudomorphs which are the products of a complete replacement of K-feldspar (Figs. 2D, 5C and 5D).

Albite overgrowths have a white and clear appearance under the conventional light microscope. They appear as euhedral crystals, predominately on dissolved K-feldspar, on non-altered oligoclase and albitized feldspar (Figs. 2A, 5A-5B). The albite overgrowths partly cover cloudy

albitized K-feldspar grains and oligoclase, and show dull luminescence (Fig. 5A). Apart from the occurrence as overgrowth on feldspar surfaces, albite also occurs as euhedral crystals together with rhombohedral siderite in secondary pores of dissolved K-feldspar (Fig. 2C). These albite crystals are oriented parallel with the cleavages of dissolved K-feldspar (Fig. 2C). Albite overgrowth and albite euhedral crystals in dissolved K-feldspar are dense without pores or inclusions, and lack twinning.

Albite patches/pseudomorphs have a sharp edge/surface and a dark-blurred appearance under the conventional light microscope due to high porosity and the presence of fine-crystalline pyrite (Fig. 5C). In some cases, mica particles and fluid inclusions can even be found in replacive albite patches. In strongly altered feldspar grains/albite patches (not in full pseudomorphs), the K-feldspar relicts can be found (Figs. 5B, 5D). It is noteworthy that the replacive albite patches have dull luminescence while the K-feldspar relicts appear with a light yellow under cathodoluminescence (Fig. 5D).

Detailed SEM investigations reveal that the albite crystals in the Magnus sandstones have unetched smooth surfaces, and were observed on altered K-feldspar (Fig. 2E). Besides, a pseudomorphous replacement of feldspar by relatively large blocky crystals of albite occurs. Albite also appears as overgrowth partly coating detrital K-feldspar/oligoclase (Fig. 2F).

5.3 Chemical composition of feldspar

Based on the chemical composition, feldspar can be divided into three groups: K-feldspar, oligoclase and albite (Fig. 6). Within the K-feldspar group, the K-feldspar relicts in albitized grains have a narrow range of chemical compositions compared with the unaltered, fresh K-feldspar (Fig. 6A). Oligoclase commonly appears unaltered and has a 20-30% An (anorthite)

content. In general, the investigated albite in the Magnus sandstones is close to pure albite. However, the three forms of albite have different chemical compositions (Fig. 6B). The albite overgrowth has the highest purity in view of the chemical composition, with 100% Ab (Fig. 6B). However, the albite lamellae and the albite patches are less pure. The albite lamellae in perthite in the Magnus sandstones are composed of 2-4% An whereas the albite patches/pseudomorphs have a chemical composition range of 1-3% An.

6. Discussion

6.1 Origin of albite

Diagenetic albite in siliclastic sedimentary rocks has several chemically and petrographically characteristic features: (1) compositional purity (99% Ab), (2) cloudy or vacuolised appearance in thin sections, (3) untwined crystallinity, and (4) a lack of cathodoluminescence (Smith and Stenstrom, 1965; Kanster, 1971; Kanster and Siever, 1979; Saigal et al., 1988).

Albite overgrowth in the Magnus sandstones has an undoubtedly diagenetic origin due to its fresh surface, dull luminescence, and high purity (100% Ab). However, the origin of replacing albite patches, especially as albite pseudomorphs, which are the products of a complete replacement of K-feldspar, is obscured. Besides the unaltered appearance of the albite patches (Fig. 5C), there are further lines of evidence that suggest that the albite patches in the studied sandstones have formed during diagenesis. First, the albite patches are observed in the dissolved part of K-feldspar and the dissolved K-feldspar still maintains its original shape (Fig. 2D). This suggests that the formation of albite patches postdated K-feldspar dissolution and that the dissolution of K-feldspar took place during burial after compaction. Second, the replacing albite patch is absent at the contacts of altered feldspar grains and quartz overgrowth, and its shape

follows the edge of quartz overgrowth (Figs. 2A, 5D), indicating that albite patch may postdate quartz overgrowth.

However, a derivation from the source rocks which contain albitized feldspar as another origin for the albite patches type of the Magnus sandstones cannot be fully excluded. First, the chemical composition of the albite patches is 95-98% Ab, which is slightly less pure than the criteria of 99% Ab suggested by Saigal et al. (1988). Second, the cloudy albite patches also share many similarities with albite formed in granitic rocks described by Engvik et al. (2008; Fig. 4): cloudy appearance due to numerous pores, fine inclusions of mica, pyrite or Fe-oxide, and slight impurity (An_{2-5}). Third, the Na_2O contents of albite and the bulk albite contents in the studied well both show an increase trend with increasing feldspar amount and decreasing grain size (Figs. 4D, 4F). There are two explanations for this phenomenon: albite as allochthonous component was preferentially deposited in small grain-sized sandstones, or formed especially in small grain-sized sandstones. The first explanation is more likely for the Magnus sandstones. Odom et al. (1976) found out that the feldspar contents decrease with increasing grain size based on the investigation of sandstones of Cambrian, Ordovician, Permian and Jurassic age. They concluded that the high concentration of feldspars in fine sandstones is a result of sorting of feldspar in contiguous high energy environments. In the Magnus sandstones, the relative abundance of feldspar in fine grain-sized sandy units is also observed (Fig.4D). Coupled to the more feldspar in small grain-sized sandstone, the albite contents in these samples are also relatively abundant (Fig. 4D). If the albite content in small grain-sized sandstones was exclusively due to the formation of authigenic albite, then an increased Na/K ratio should be expected in albite-rich, fine grain-sized samples due to an addition of sodium during the formation of albite. However, the plots of Na_2O and K_2O values display a linear relationship

(Fig.4C), which suggests an instant Na_2O/K_2O value in all studied samples. In addition, the K-feldspar contents of the Magnus sandstones do not decrease with the increased albite abundance whereas they increase with increased albite contents (Fig. 4D), which indicates the albite in the Magnus sandstones might not be exclusively due to the replacement of K-feldspar. It seems that albite, probably a large portion, is linked to albitized parent rocks which were albitized, eroded and transported to the present area of the Magnus field.

Based on this discussion, two origins can be argued to the albite in the Magnus sandstones: detrital albitized grains as inherited from the parent rocks and diagenetic albite during burial.

6.2 Timing of diagenetic albite formation

Diagenetic albite of the Magnus sandstones was formed during burial to great depths. Several petrographic observations can support this hypothesis as below: (1) fresh albite occurring in corroded K-feldspar grains which still keep their original skeleton (Figs. 2C, 2D), indicating that albite formation postdated compaction and K-feldspar-dissolution; (2) the absence of replacing albite at contacts of detrital grains and quartz overgrowth (Figs 2A, 5C, and 5D); (3) albite overgrowth followed the shape of quartz overgrowth (Fig. 2A), suggesting that albite formed after quartz overgrowth. In summary, authigenic albite formation, or at least partly, postdated mechanical compaction, K-feldspar dissolution and quartz cementation. Since the formation of the diagenetic albite is later than quartz cementation, the timing of quartz cementation can be regarded as the earliest time for diagenetic albite formation. The age of quartz cementation was assessed to be 80 Ma based on the homogenization temperature of aqueous inclusions of 90-120°C measured in the quartz cement and on the burial history of the Magnus sandstones (Emery et al., 1993; Fig 7). Therefore, it can be inferred that the earliest age for diagenetic albite in the

Magnus sandstones could be 80 Ma when the reservoir temperature could have been around 90°C (Fig. 7). Albite formation seems to be still proceeding in the present Magnus sandstones, since most of today's formation waters of the Magnus field fall in the stability field of albite by plotting the formation waters data form Warren and Smalley (1994) on the stability diagram of Morad et al. (1990).

6.3 Chemical conditions required for albitization

6.3.1 Source of sodium

One of the chemical conditions required for authigenic albite formation is a high activity ratio of Na^+/H^+ in combination with a high concentration of dissolved silica (H_4SiO_4) (Karster and Siever, 1979). The source of Na^+ ions may originate from the pore water. Given 2 wt. % albite is formed in the Magnus sandstones (assuming porosity 20%, density: 2.65 mg/cm^3), a pore water with a salinity of 18,630 mg/L sodium is needed for the sodium supply of albite formation. The current formation water of the Magnus field has the same order of salinity with 16,000-18,000 mg/L dissolved solids (NaCl wt. % equivalents) (De'Ath and Schuyleman, 1981). Therefore, the formation water of the Magnus field can provide sufficient sodium source for the observed authigenic albite formation. An additional sodium source which exists -but maybe not necessary- is the Na^+ ion released from the transformation of smectite to illite in mudrocks of the surrounding Kimmeridge Clay Formation (*cf.* Boles and Franks, 1979). Moreover, the alkali feldspar in the Magnus sandstones contains 2-10% Ab and dissolution of such alkali feldspar can supply some additional sodium for albite formation.

6.3.2 Source of silica

The source of silica can either come from skeletal organisms or from dissolution of unstable silicate grains (Karster and Siever, 1979). Silica-bearing skeletal organisms have not been observed or reported in the Magnus sandstones.

However, dissolution of unstable silicates, such as non-end-member feldspars, can also supply dissolved silica. Intermediates in either the plagioclase or alkali feldspar series are less stable than the pure end members at low temperature (Milliken, 2004). The non-end-member alkali feldspar in the Magnus sandstones accounts for 8-14 wt. % of the whole rock and is composed with 2-10% Ab (Fig. 6). Dissolution of K-feldspar is common in the Magnus sandstones (Figs. 2C, 2D, and 2E). Thus, dissolution of non-end member K-feldspar is the possible source for elevated dissolved H_4SiO_4 concentrations in the Magnus sandstones. In addition, it can also provide sodium by the following reaction:

$$K_{0.9}Na_{0.1}AlSi_3O_8 + 4H^+ + 4H_2O \rightarrow 0.9K^+ + 0.1Na^+ + Al^{3+} + 3H_4SiO_4 \quad [1]$$

6.3.3 Potassium sink

Albitization is more sensitive to potassium removal than sodium supply (Aagaard et al., 1990). It is envisaged that the adjoining and interbedded shales within sandstone sequences provide an effective potassium sink for albitization (Saigal et al., 1988; Aagaard et al., 1990), since the change of smectite into illite can consume potassium and release sodium (Boles and Franks, 1979). In addition, the alteration of kaolinite to illite in sandstones and shales would also remove potassium (Bjorlykke et al., 1995; Bjorlykke, 1998). In the Magnus field, illite formation in the Magnus sandstones has been reported by Worden and Barclay (2003) and they interpreted that its formations is related to dissolution of K-feldspar and kaolinite (see also Fig. 2G). In addition, illite is not only present in sandstones (1-2 wt. %; Fig. 3), but also occurs in the interbedded

shales (5-15 wt. %; Fig. 3). Therefore, it can be inferred that illite in the shales of the Kimmeridge Clay Formation and in the Magnus sandstones is the likely potassium sink for diagenetic albite formation.

7. Hydrogeochemical modelling of albite formation

7.1. Geological framework and input parameters

Authigenic albite formation in the Magnus sandstones is interpreted to have occurred during burial (section 6.2). Correspondingly, several scenarios aim to test the possible pathways for authigenic albite formation. The sediments of the Magnus field have experienced a burial history of multiple uplifts and erosions, long term weathering, and meteoric water flushing (sections 3 and 6.2). During uplift and shallow overburden, several diagenetic processes occurred, including dissolution of unstable feldspars and precipitation of kaolinite and chalcedony. During this period, oxidizing conditions should have prevailed in the Magnus sandstones and resulted in formation of hydrous ferric oxides (HFO). Besides the observed detrital minerals of the Magnus sandstones (quartz, K-feldspar, and probably also albitized grains), additional minerals such as kaolinite, chalcedony, hydrous ferric oxide (HFO) are also considered to be present in the Magnus sandstones after early diagenesis (this part is excluded in our study and modelling), as the primary minerals for modelling the following continuous burial diagenetic processes.

Increasing in temperature and pressure during burial could change the solubility constant of minerals. Consequently, it should be taken into account as a possible reason for authigenic albite formation (scenario 1).

Scenario 2 considers organic-inorganic interactions during albite formation. Siderite is present together with authigenic albite (Fig. 2C). However, the petrographic investigations show that the

Magnus sandstones lack organic matter which may serve as reductant for ferric iron to enable siderite formation. Before and during oil generation, several reactive components could also be produced, like methane and carbon dioxide (Tissot et al., 1974, 1978; Hunt, 1995). These products could have migrated into the Magnus sandstones before oil migration or together with oil. In the presence of pore water and other mineral oxidants, oil components are unstable in view of chemical thermodynamics and can be degraded into methane, carbon dioxide, carboxylic acid and hydrogen (Seewald, 2003). These reactive products may have enabled electron transfer for siderite formation. This hypothesis is also supported by the results of former studies that found that siderite in the Magnus sandstones was formed at 90 °C coupled with oil generation and migration (Macaulay et al., 1993b; Emery et al., 1993) and that its carbon isotopic composition ($\delta^{13}C$ of -8.0 to -14.6‰ PDB; Macaulay et al., 1993b) reflects an important influence of organic matter sourced carbon. During the transformation of ferric iron to ferrous iron minerals, the pH and redox conditions of pore water could have changed. This could have triggered a series of other diagenetic processes. The second scenario thus aims to test whether albite formation could have occurred coupled to siderite formation in the period of oil generation and migration into the Magnus sandstones during the second and major burial phase.

Illite formation at the expense of K-feldspar and kaolinite is commonly observed in North Sea oil reservoirs, and is controlled by kinetics (Bjorlykke et al., 1995; Bjorlykke, 1998; Worden and Barclay, 2003). The formation waters of the North Sea oil reservoirs are undersaturated with regard to K-feldspar, and, instead, oversaturated with regard to illite and albite (Bjorlykke et al., 1995). As mentioned in section 6.3.3, illite formation and K-feldspar dissolution are also commonly observed in the Magnus sandstones (Fig. 2H). Dissolution of such non-end-member K-feldspar of the Magnus sandstones can also release sodium ions into the pore water.

Consequently, this leads to an albite oversaturation and precipitation. The third scenario thus aims to test whether this process is thermodynamically admissible in the mineralogical assemblage of the Magnus sandstones. Thus, this kinetic process is not considered in the first and second scenarios that are calculated under chemical equilibrium conditions.

7.2. Modelling concept

To test the three possible pathways for albite formation in the Magnus sandstones, a hydrogeochemical batch modelling approach, which is based on thermodynamics of chemical equilibrium, is presented. The computer code Phreeqc Interactive 3.2 that was developed by the U.S. Geological Survey (Parkhurst and Appelo, 2013) is our modelling tool. Table 3 shows the potential amounts of primary and secondary minerals and the current temperature and pressure conditions in the sandstones of the Magnus oilfield. Since the primary detrital minerals have been strongly altered, their original amounts prior to burial can only be assumed according to the petrographic observations. Assuming an initial porosity of 20 % based on petrographic investigations, our modelling approach consists of a generic reactor that has a total volume of 5 L. One liter of the present-day seawater, which is documented in the Phreeqc Manual (Parkhurst and Appelo, 2013), fills the pore space of this reactor. According to an average density of 2.65 g/L, the reactor has a mineral assemblage with a total mass of 10.6 kg. The pre-assigned mineral assemblage for modelling and their amounts are given in Table 3. Although quartz predominates in the mineral assemblage, it is conceptually only allowed to dissolve. Instead, chalcedony may form as secondary $SiO_{2(s)}$ as it commonly occurs in form of small crystals and overgrowths. In general, less stable $SiO_{2(s)}$ minerals, such as chalcedony and cristobalite, control the concentration of dissolved silica in aqueous solutions, whereas these solutions are oversaturated

with respect to quartz (Appelo and Postma, 1994). K-feldspar and albite, the main sedimentary minerals besides quartz, account for 8 and 12 wt.-% of the sedimentary mineral assemblage of the sandstones, respectively (Table 3).

7.3. Modelling results

Scenario 1 uses an assumed temperature-pressure gradient according to the present conditions (4 to 116 °C in 10 steps; 1 to 450 atm in 10 steps; Phreeqc input file in Appendix). The results (not graphically shown) suggest that the pre-assigned mineral assemblage is stabilized with increasing temperature and pressure conditions, because negligible amounts of minerals are converted in the modelling (mostly in the order of magnitude of 10^{-4} mol per one liter of pore water). Additionally, albite is slightly dissolved (5E−4 mole per one liter of pore water). Thus, an increase in temperature and pressure, which changes the solubility constants of minerals including K-feldspar and albite, is not the reason for albite formation under isochemical conditions.

Scenario 2 considers a stepwise addition of the oil generation/degradation products methane, carbon dioxide, and hydrogen according to Seewald (2003). In total, 0.007 moles of CO_2, CH_4 and H_2 in a 2:1:5 ratio are added into the reactor in 10 steps, until the assumed amount of ferric iron minerals is completely consumed (scenario 2 input file in Appendix). The modelling results show that the pH of the pore water gradually increases whereas E_H decreases (Fig. 8A). These changes lead to reduction of hydrous ferric oxide and siderite formation. During this process, K-feldspar remains stable, and up to 1.5 wt. % albite can form (Fig. 8B). However, the modelled K-feldspar stability does not match the common dissolution features of K-feldspar observed in the Magnus sandstones. However, K-feldspar dissolution may have occurred during uplift and

erosion due to the infiltration of meteoric water. Moreover, kaolinite and chalcedony dissolve in scenario 2. In comparison, precipitation of kaolinite and quartz overgrowth are proven by SEM and optical microscopy. However, this conflict may not doubt the modelling approach, because the observed kaolinite and quartz overgrowth may have formed during uplift and erosion stages which are not included in our modelling concept.

Scenario 3 aims to test the third hypothesis: whether the kinetic transformation from non-end member K-feldspar with Ab_{10} altering to illite can lead to albite formation. This scenario considers a stepwise addition of a K-feldspar with Ab_{10} into the reactor in order to simulate the kinetic-controlled transformation from K-feldspar to illite (scenario 3 input file in Appendix). It is assumed that this K-feldspar has same thermodynamic data as the pure K-feldspar defined in the Phreeqc database. The modelling results show that dissolution of non-end member K-feldspar is coupled to a formation of albite, illite, and chalcedony (Fig. 8D). In parallel, kaolinite is consumed. This fits the SEM observations that illite is precipitated on the surface of kaolinite (Fig. 2G). Due to the low sodium content in the non-end member K-feldspar, only 0.034 wt. % albite can be precipitated, while 1 wt. % illite is formed (Fig. 8D). In comparison, the measured data show that ca. 2 wt. % albite and 1 wt. % illite are formed. Even though a difference exists between the modelled and measured illite/albite ratio, our modelling results suggest that the illite formation via the kinetic transformation of non-end member K-feldspar can lead to albite formation in view of chemical thermodynamics.

In summary, two alternative pathways may have led to authigenic albite formation. However, an overall valid explanation and thus exclusive pathway for the authigenic albite formation in the Magnus sandstones cannot be inferred. Thus, it is likely that selected parts of these two pathways may contribute to the complex and interacting process chain together for the albite formation in

the Magnus sandstones.

8. Conclusions

(1) Up to 18 wt. % albite occurs in the Magnus sandstones and its contents vary with depth and correlate with increasing K-feldspar content and increasing grain size.

(2) Albite occurs as lamellae in perthite, as overgrowth on dissolved K-feldspar and/or replacive patches in altered K-feldspar grains. All kinds of albite in the Magnus sandstones have dull cathodoluminescence and a high purity of chemical composition. Especially, the albite overgrowth is pure (100% Ab), and differs from albite lamellae with 2-4% An and replacing albite patches with 1-3% An.

(3) A part of albite can be inferred as diagenetic albite based on unaltered crystal surfaces, its high purity, and dull cathodoluminiscence as well as its co-occurrence with other diagenetic minerals.

(4) Diagenetic albite was formed during burial, K-feldspar dissolution and quartz cementation. The initial start of diagenetic albite formation in the Magnus sandstones could be 80 Ma BP and it may continue to form until today. Correspondingly, the temperature range for the diagenetic albite formation in the Magnus sandstones is 90-120°C.

(5) Hydrogeochemical modelling indicates that an increase in temperature and pressure as major control is not the reason for albite formation. Two possible pathways for authigenic albite formation in the Magnus sandstones are presented and discussed: (i) dissolution of kaolinite and chalcedony coupled with reduction of ferric iron minerals by reducing agents produced during oil generation, migration and degradation, and (ii) dissolution of non-end member K-feldspar.

Acknowledgements

Funding of Nana Mu was provided by the Chinese Scholarship Council (CSC). The authors thank the British Geological Survey for access to core samples, and Laura González Acebrón and an anonymous reviewer for their constructive and helpful comments.

References

Aagaard, P., Egeberg, P.K., Saigal, G.C., Morad, S., Bjorlykke, K., 1990. Diagenetic albitization of detrital K-feldspars in Jurassic, Lower Cretaceous, and Tertiary clastic reservoir rocks from offshore Norway, II: Formation water chemistry and kinetic considerations. Journal of Sedimentary Petrology 60, 575–581.

Appelo, C.A.J., Postma, D., 1994. Geochemistry, Groundwater and Pollution. A.A. Balkema, Rotterdam, pp. 213–214.

Baines, S.J., Worden R.H., 2004. The long-term fate of CO_2 in the subsurface: natural analogues for CO_2 storage. In: Baines, S.J., Worden, R.H. (Eds.), Geological storage of carbon dioxide, Special Publications, 233. The Geological Society of London, London, pp. 59–86.

Barclay, S.A., Worden, R.H., 1998. Quartz cement volumes across oil-water contacts in oil fields from petrography and wireline logs: preliminary results from the Magnus Field, Northern North Sea. In: Harvey, P.K., Lovell, M.A. (Eds.), Core-log integration, Special Publications 136. The Geological Society of London, London, pp. 327–339.

Barclay, S.A., Worden, R.H., 2000. Geochemical modelling of diagenetic reactions in a sub-arkosic sandstone. Clay Minerals 35, 57–57.

Barclay, S.A., Worden, R.H., Parnell, J., Hall, D.L., Sterner, S.M., 2000. Assessment of Fluid Contacts and Compartmentalization in Sandstone Reservoirs Using Fluid Inclusions : An Example from the Magnus Oil Field, North Sea. AAPG Bulletin 84, 489–504.

Bjorlykke, K., 1998. Clay mineral diagenesis in sedimentary basins: a key to the prediction of rock properties, examples from the North Sea Basin. Clay Minerals 33, 15–34.

Bjorlykke, K., Aagaard, P., Egeberg, P.K., Simmons, S.P., 1995. Geochemical constraints from formation water analyses from the North Sea and Gulf Coast Basin on quartz, feldspar and illite precipitation in reservoir rocks. In: Cubitt, J.M., England, W.A. (Eds.), The Geochemistry of Reservoirs, Geochemical Soc. Spec. Pub., 86, pp. 33–50.

Boles, J.R., 1982. Active albitization of plagioclase. Gulf Coast Tertiary. American Journal of Science 282, 165–180.

Boles, J.R., Franks, S.G., 1979. Clay diagenesis in Wilcox sandstones of southwestern Texas: implications of smectite diagenesis on sandstone cementation. Journal of Sedimentary Petrology 49, 55–70.

Bozau, E., Sattler, C-D., van Berk, W., 2015. Hydrogeochemical classification of deep formation waters. Applied geochemistry 52, 23–30.

De'Ath, N.G., Schuyleman, S.F., 1981. The geology of Magnus oilfield. In: Illing, L.V., Hobson, G.D. (Eds.), Petroleum geology of the continental shelf of the north-west Europe, Heyden, London, pp. 342–351.

Ehrenberg, S.N., Jacobsen, K.G., 2001. Plagioclase dissolution related to biodegradation of oil in Brent Group sandstones (Middle Jurassic) of Gullfaks Field, northern North Sea. Sedimentology 48, 703–722.

Emery, D., Myers, K., Young, R., 1990. Ancient subaerial exposure and freshwater leaching in

sandstones. Geology 18, 1178-1181.

Emery, D., Smalley, P.C., Oxtoby, N.H., Ragnarsdottir, K.V., Aagaard, P., Halliday, A., Coleman, M.L., Petrovich, R., 1993. Synchronous Oil Migration and Cementation in Sandstone Reservoirs Demonstrated by Quantitative Description of Diagenesis [and Discussion]. Philosophical Transactions of the Royal Society A: Mathematical, Physical and Engineering Sciences 344, 115-125.

Engvik, A.L., Putnis, A., Fitz Gerald, J.D., Austrheim, H., 2008. Albitization of granitic rocks: the mechanism of replacement of oligoclase by albite. Canadian Mineralogist 46, 1401-1415.

Gold, P.B., 1987. Textures and geochemistry of authigenic albite from Miocene sands, Louisiana Gulf Coast. Journal of Sedimentary Petrology 57, 353-362.

González-Acebrón, L., Arribas, J., Mas, R., 2010. The role of sandstone provenance in diagenetic albitization of feldspars. A case study in the Jurassic Tera Group sandstones (Cameros Basin, NE Spain). Sedimentary Geology 229, 53–63.

Helgeson, H. C., Knox, A. M., Owens, D. H., Shock, E. L., 1993. Petroleum, oil-field waters, and authigenic mineral assemblages – are they in metastable equilibrium in hydrocarbon reservoirs. Geochim. Cosmochim. Acta 57, 3295–3339.

Hirt, W.G., Wenk, H-R., Boles, J.R., 1993. Albitization of plagioclase crystals in the Stevens sandstone (Miocene), San Joaquin Basin, California, and the Frio Formation (Oligocene), Gulf Coast, Texas: a TEM/AEM study. Geological Society of America Bulletin 105, 708–714.

Hunt, J.M., 1995. Petroleum Geochemistry and Geology, Second edition. W.H. Freeman and Company, New York.

Kastner, M., 1971. Authigenic feldspars in carbonate rocks. American Mineralogist 56, 1403-1442.

Kastner, M., Siever, R., 1979. Low temperature feldspars in sedimentary rocks. American Journal of Science 279, 435–479.

Macaulay, C., Fallick, A., Haszeldine, R., 1993a. Textural and isotopic variations in diagenetic kaolinite from the Magnus Oilfield Sandstones. Clay minerals 28, 625–639.

Macaulay, C., Haszeldine, R., Fallick, A., 1992. Diagenetic pore waters stratified for at least 35 Million Years: Magnus oil field, North Sea. AAPG 76, 1625–1634.

Macaulay, C., Haszeldine, R., Fallick, A., 1993b. Distribution, chemistry, isotopic composition and origin of diagenetic carbonates: Magnus Sandstone, North Sea. Journal of Sedimentary Research 63, 33–43.

Milliken, K.L., Land, L.S., Loucks, R.G., 1981. History of burial diagenesis determined from isotopic geochemistry, Frio Formation, Brazoria County, Texas. AAPG Bulletin 65, 1397–1413.

Milliken, K.L., 1989. Petrography and composition of authigenic feldspars, Oligocene Frio Formation, South Texas. Journal of Sedimentary Petrology 59, 361–374.

Milliken, K.L., 2004. Late diagenesis and mass transfer in sandstones-shale sequences. In: Mackenzie, F.T. (Eds.), Sediments, Diagenesis, and Sedimentary Rocks: Treatise on Geochemistry. Elservier-Pergamon, Oxford, UK, 7, pp.159–190.

Morad, S., Bergan, M., Knarud, R., Nystuen, J.P., 1990. Albitization of detrital plagioclase in Triassic reservoir sandstones from the Snorre Field, Norwegian North Sea. Journal of Sedimentary Petrology 60, 411–425.

Odom, I.E., Doe, T.W., Dott, R.H., 1976. Nature of feldspar-grain size relations in some quartz-

rich sandstones. Journal of Sedimentary Petrology 46, 862–870.

Parkhurst, D.L., Appelo, C.A.J., 2013. Description of input and examples for PHREEQC Version 3–A computer program for speciation, batch-reaction, one-dimensional transport, and inverse geochemical calculations. U.S. Geological Survey Techniques and Methods, book 6, chapter A43, available only at http://pubs.usgs.gov/tm/06/a43/.

Pittman, E.D., 1988. Diagenesis of Terry sandstone (Upper Cretaceous), Spindle Field, Colorado. Journal of Sedimentary Petrology 58, 785–800.

Saigal, G.C., Morad, S., Bjorlykke, K., Egeberg, P.K., Aagaard, P., 1988. Diagenetic albitization of detrital K-feldspar in Jurassic, Lower Cretaceous, and Tertiary clastic reservoir rocks from offshore Norway, I. Textures and origin. Journal of Sedimentary Petrology 58, 1003–1013.

Seewald, J.S., 2003. Organic-inorganic interactions in petroleum-producing sedimentary basins. Nature 426, 327–333.

Shepherd, M., 1991. The Magnus Field, Block 211/7a, 12a, UK North Sea. Geological Society, London, Memoirs 14, 153–157.

Smith, J.V., Stenstrom, R.C., 1965. Electron-excited luminescence as a petrologic tool, Geology 73, 627-63.

Surdam, R.C, Crossey, L.J., Hagen, E.S., Heasler, H.P., 1989. Organic-inorganic interactions and sandstone diagenesis. AAPG Bulletin 73, 1–23.

Tissot, B., Durand, B., Espitalie, J., Combaz, A., 1974. Influence of nature and diagenesis of organic matter in formation of petroleum. AAPG Bulletin 58, 499–506.

Tissot, B.P., Welte, D.H., 1978. Petroleum Formation and Occurrence: A New Approach to Oil and Gas Exploration. Springer-Verlag, Berlin, pp. 538.

Walker, T.R., 1984. Diagenetic albitization of potassium feldspar in arkosic sandstones. Journal of Sedimentary Petrology 54 (1), 3–16.

Warren, E.A., Smalley, P.C., 1994. The Magnus field. In: Warren, E.A., Smalley, P.C. (Eds.), North Sea formation waters atlas. Memoir No. 15. The Geological Society, London, pp.51.

Worden, R.H., Barclay, S.A., 2000. Internally-sourced quartz cement due to externally-derived CO_2 in sub-arkosic sandstones, North Sea. Journal of Geochemical Exploration 69-70, 645–649.

Worden, R.H., Barclay, S.A., 2003. The effect of oil emplacement on diagenetic clay minerology: the Upper Jurassic Magnus Sandstone Member, North Sea. In: Worden, R.H., Morad, S. (Eds.), Clay minerals in sandstones. Blackwells, Oxford, UK, pp. 453–469.

Figure captions

Figure 1. (A) Location map of the Magnus oilfield, the sampled well (211/12a-9) and cross section A-B shown in figure B. (B) Cross section of the Magnus oilfield, which shows the intercalation of the Magnus Sandstone Member between the Upper and Lower Kimmeridege Clay Formations (UKCF, LKCF) below the mid-Cretaceous unconformity.

Figure 2. Main diagenetic features of the Magnus sandstones. (A) The altered K-feldspar with partly coated albite overgrowth (white arrow). The edge/boundary of albite overgrowth of the right grain following the shape of quartz overgrowth (black arrow). Both corroded and non-corroded K-feldspars occur. Ankerite and kaolinite fill pores; // nicols. (B) Siderite and ankerite cement; BSE. (C) Authigenic albite crystals in corroded K-feldspar; BSE. (D) Authigenic albite formed within a partly corroded K-feldspar grain; BSE. The white dashed line represents the original shape of the corroded K-feldspar grain. (E) Fresh, euhedral albite crystals on corroded feldspar; SEM. (F) Albite overgrowth on detrital grains;

SEM. (G) Illite whiskers on kaolinite booklets; SEM. (H) A corroded and illitized detrital grain, BSE. The dashed lines indicate the outline of the original detrital grain which might have been feldspar. Within its skeleton, kaolinite, illite and quartz were precipitated. The insert is the EDS analysis of illite. Abbrevations: Olg: oligoclase; Q: quartz; Qo: quartz overgrowth; Kfd: k-feldspar; Alb: albite; Ill: illite; Kao: kaolinite; Ank: ankerite; Sid: siderite; Pyr: pyrite.

Figure 3. Profile of bulk rock element oxide precentages (XRF), mineral percentages (XRD) and grain size (determined by conventional light microscopy).

Figure 4. XRD and XRF results. (A) Bulk rock sodium content (from X-ray fluorescence) vs. albite content (from X-ray diffraction). The diagonal line represents correlation for ideal albite. The linear relation of Na_2O with albite indicates that albite is the predominant Na-bearing mineral. (B) Bulk rock potassium content vs. K-feldspar content. The diagonal line represents a correlation for an ideal K-feldspar. The points plotting above this line indicate the presence of other K-bearing minerals (mica, illite). (C) Bulk rock sodium content vs. bulk rock potassium content. The Na_2O content increases with increasing the K_2O content. (D) Albite content vs. K-feldspar and total feldspar contents. Albite is abundant in samples with abundant K-feldspar and total feldspar. (E) Bulk rock sodium content vs. grain size. (F) Albite and total feldspar contents vs. grain size.

Figure 5. (A) An altered black albite grain with clean albite overgrowth (arrow). The unaltered oligoclase also has a semi-coated albite overgrowth rim; // nicols. (B) Element mapping under BSE; picture as for A. Note that the albitized part has abundant micropores, pyrite and several K-feldspar relicts. (C) A black, altered K-feldspar grain under plane light. Brown kaolinite and carbonate fill part of pores; // nicols. (D) Picture as for C. The replacing albite yields dull luminescence while K-feldspar relicts show bright-yellow luminescence. Kaolinite has blue luminescence. The right quartz grain has a thick rim of quartz overgrowth with dull luminescence. Note that the right part of the replacive albite is intruded by quartz

overgrowth. The dashed lines indicate the outline of detrital quartz. The solid line represents the edge of quartz overgrowth; Cathodoluminescence. Abbrevations: Olg: oligoclase; Q: quartz; Qo: quartz overgrowth; Kfd: k-feldspar; Alb: albite; M: mica; Ca: carbonate; Kao: kaolinite.

Figure 6. Chemical compositions of feldspars in the Magnus sandstones (measured by EDS-BSE). (A) All feldspar types. (B) Albites plotting in the albite corner of former diagram (A). Note that albite overgrowth has 100% purity of Ab. Replacing albite patches are slightly impure with 1-3% An.

Figure 7. Diagenetic sequence of the Magnus sandstones (modified after Barclay et al., 2000).

Figure 8. Modelling results. (A-B) Scenario 2. (A) pH and Eh of pore water change during the addition of CH4, CO2 and H2 in each step. (B) Amount of dissolved and precipitated minerals is given in wt. %. Coupled to the dissolution of kaolinite and chalcedony, albite precipitates. (C-D) Scenario 3. (C) pH and Eh of pore water change during the addition of K-feldspar into the generic reactor. (D) Amount of dissolved and precipitated minerals is given in wt. %.

Tables

Table 1. Diagenetic features of the mineral assemblage in the Magnus oilfield.

Table 2. Characteristics of feldspars in the Magnus field.

Table 3. Present and pre-assigned mineral assemblages of the Magnus sandstones and reservoir conditions.

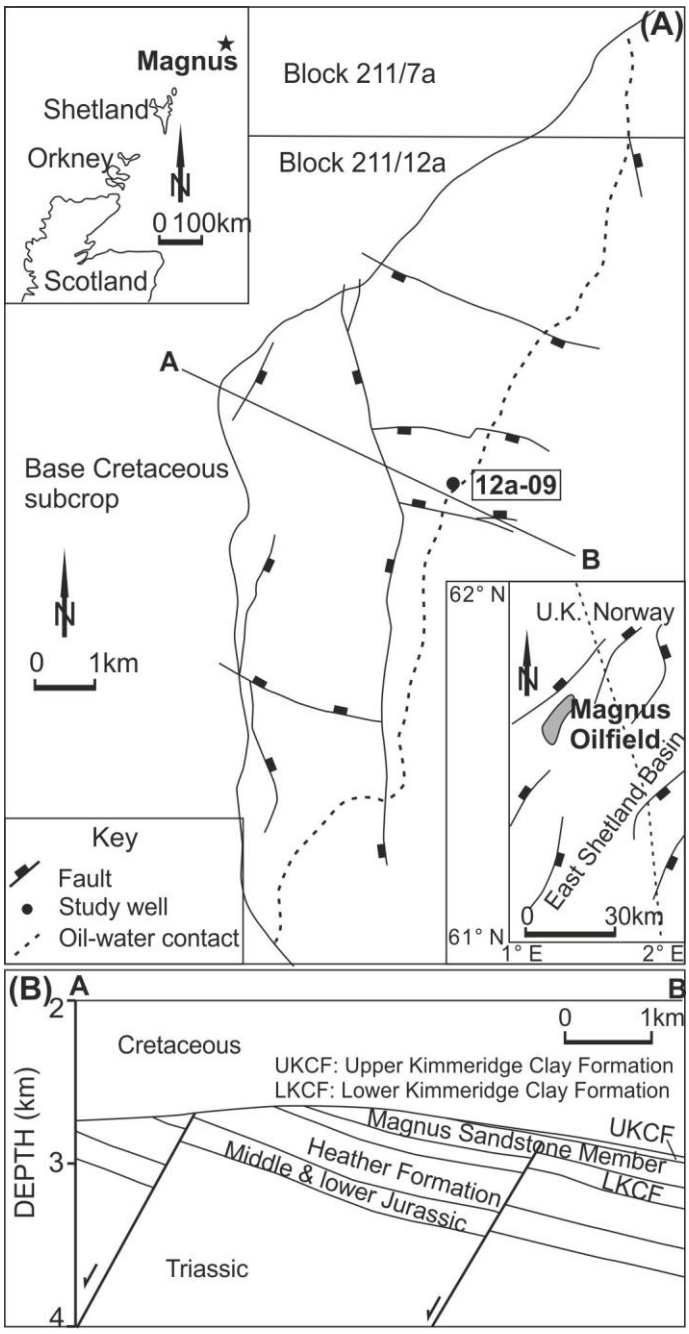
(A)
Magnus
Shetland
Orkney
Scotland
0 100km
Block 211/7a
Block 211/12a
A
B
12a-09
Base Cretaceous subcrop
0 1km
62° N
61° N
1° E
2° E
U.K.
Norway
Magnus Oilfield
East Shetland Basin
0 30km
Key
Fault
Study well
Oil-water contact
(B)
A
B
0 1km
Cretaceous
UKCF: Upper Kimmeridge Clay Formation
LKCF: Lower Kimmeridge Clay Formation
DEPTH (km)
2
3
4
UKCF
Magnus Sandstone Member
LKCF
Heather Formation
Middle & lower Jurassic
Triassic

Figure 1.

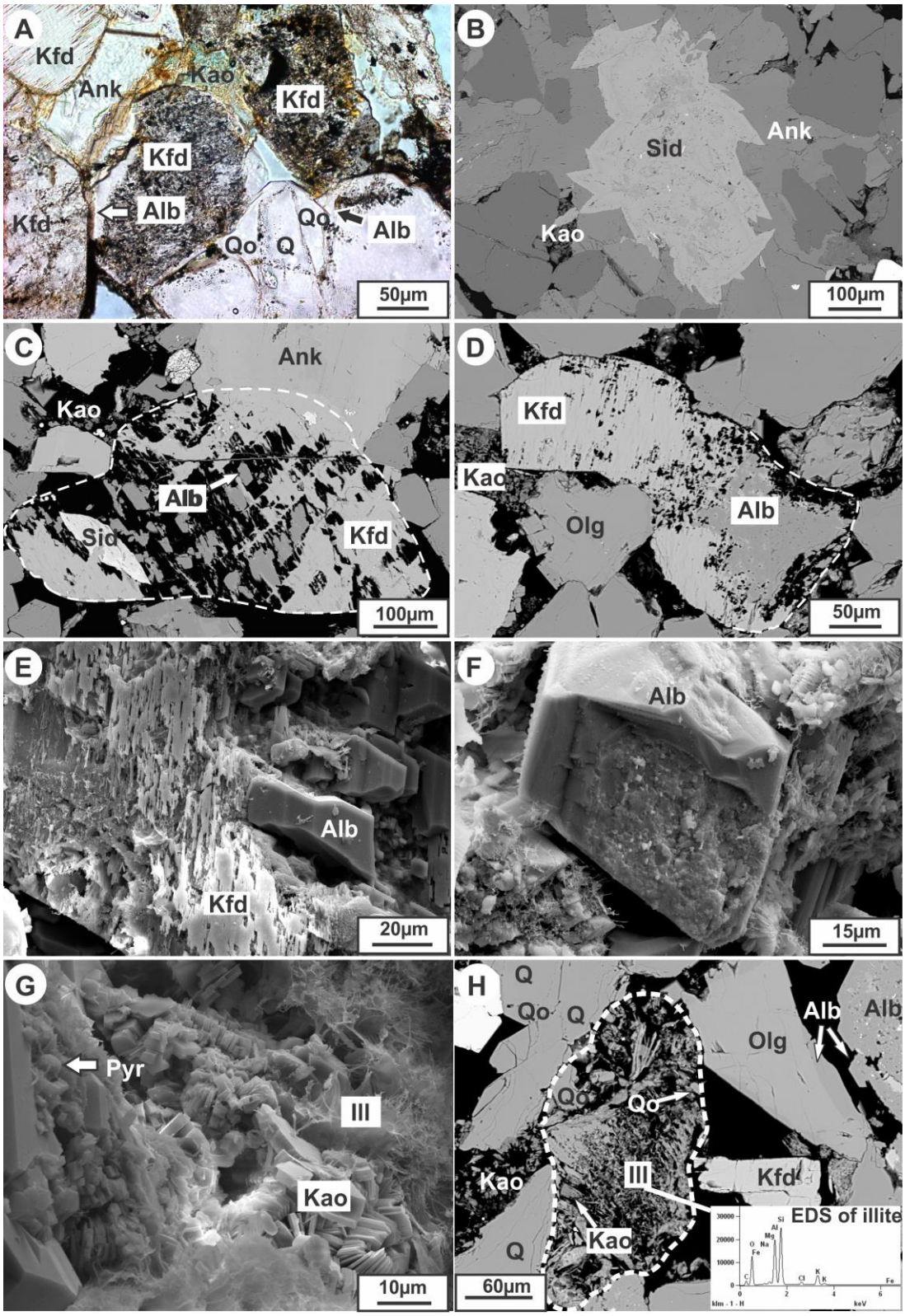
A
Kfd
Ank
Kao
Kfd
Kfd
Alb
Kfd
Qo
Alb
Qo
Q
50μm
B
Sid
Ank
Kao
100μm
C
Ank
Kao
Alb
Sid
Kfd
100μm
D
Kfd
Kao
Olg
Alb
50μm
E
Alb
Kfd
20μm
F
Alb
15μm
G
Pyr
III
Kao
10μm
H
Q
Qo
Q
Alb
Alb
Olg
Qo
Qo
Kao
III
Kfd
Kao
Q
EDS of illite
60μm

Figure 2.

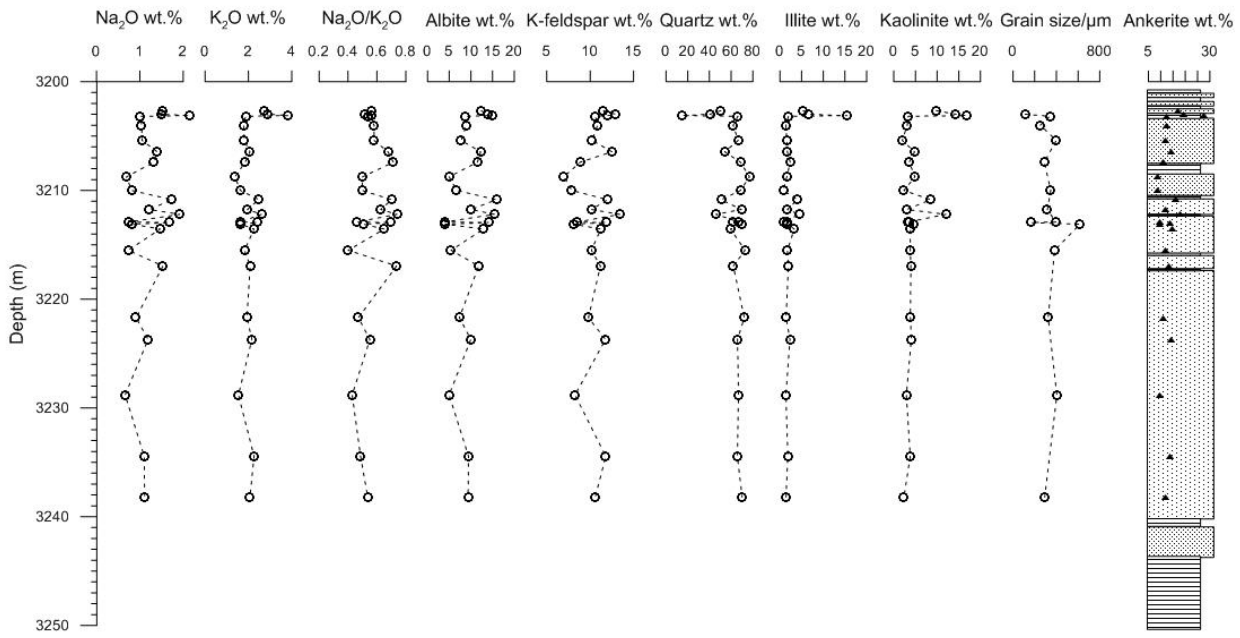
Na2O wt.%
K2O wt.%
Na2O/K2O
Albite wt.%
K-feldspar wt.%
Quartz wt.%
Illite wt.%
Kaolinite wt.%
Grain size/μm
Ankerite wt.%
Depth (m)
3200
3210
3220
3230
3240
3250

Figure 3.

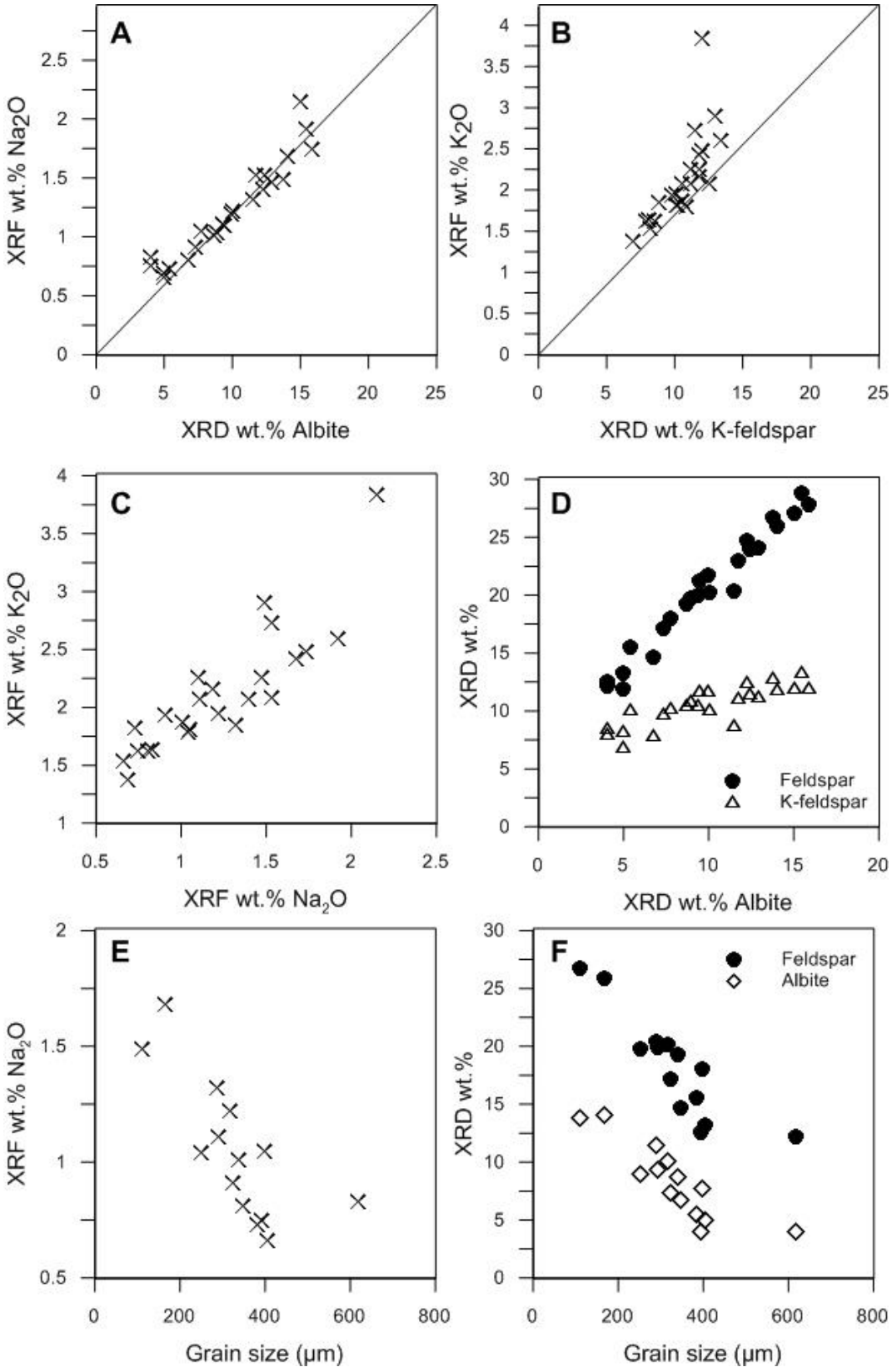
A
XRF wt.% Na2O
XRD wt.% Albite
B
XRF wt.% K2O
XRD wt.% K-feldspar
C
XRF wt.% K2O
XRF wt.% Na2O
D
XRD wt.%
Feldspar
K-feldspar
XRD wt.% Albite
E
XRF wt.% Na2O
Grain size (μm)
F
XRD wt.%
Feldspar
Albite
Grain size (μm)

Figure 4.

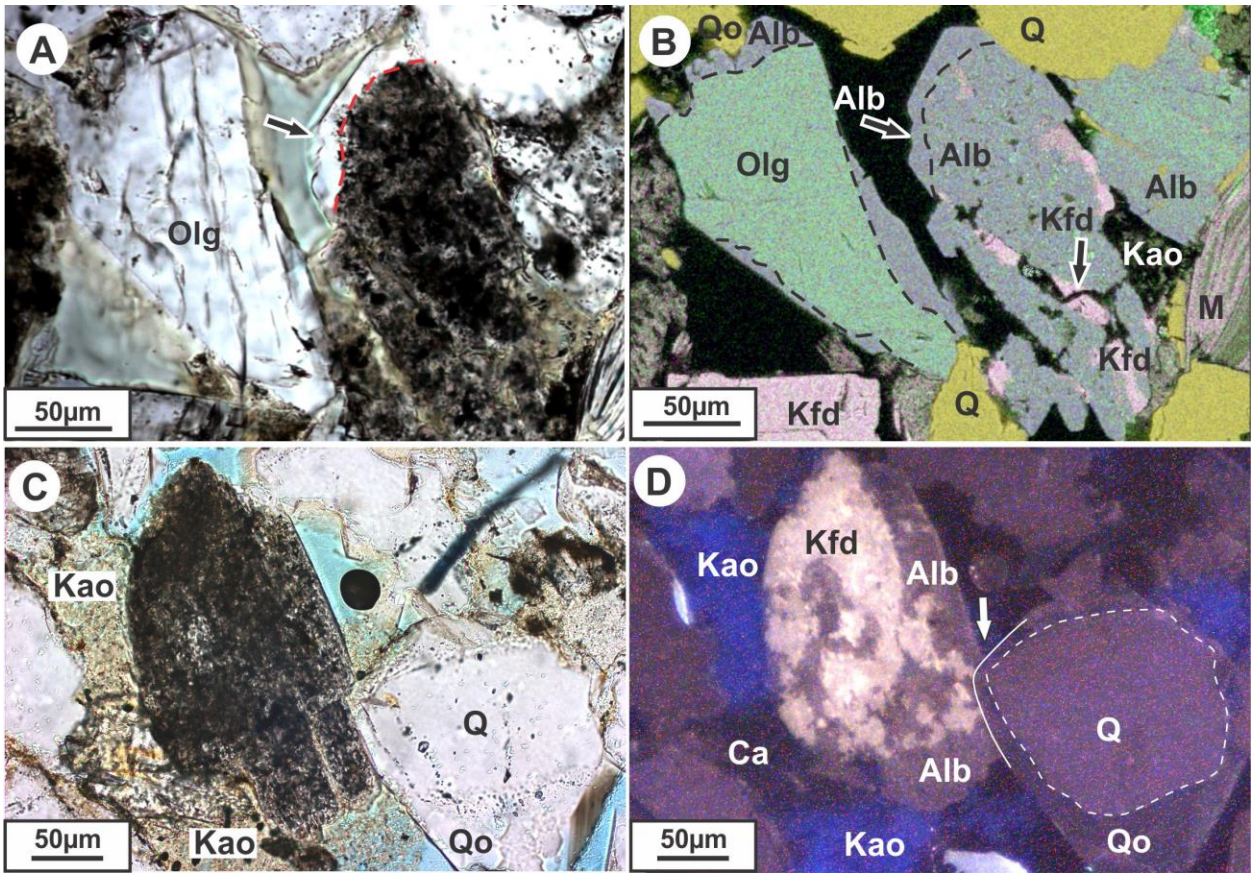

Figure 5.

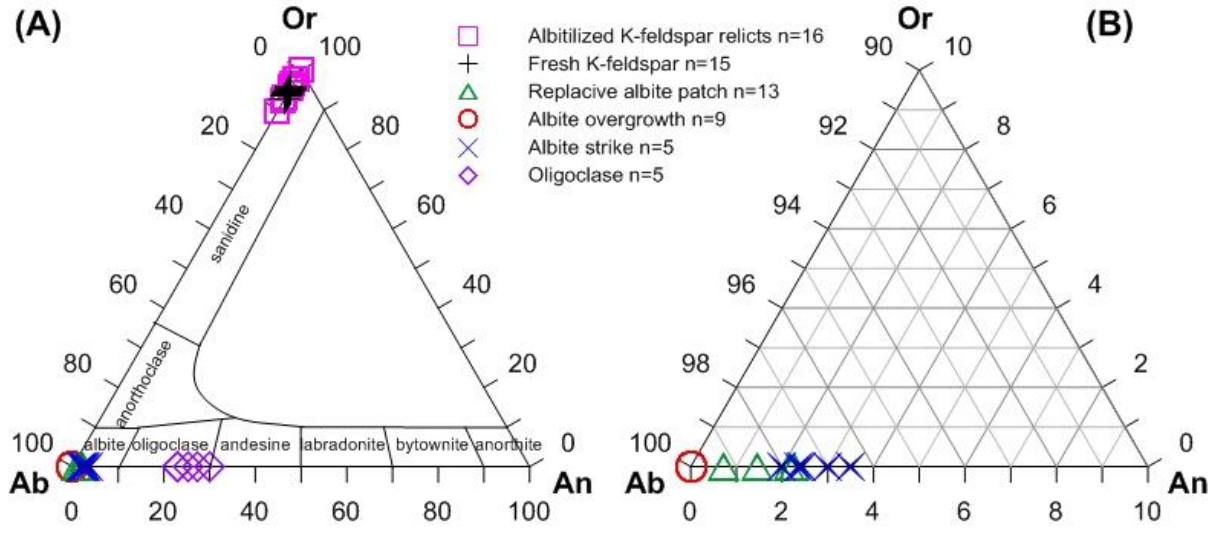

Figure 6.

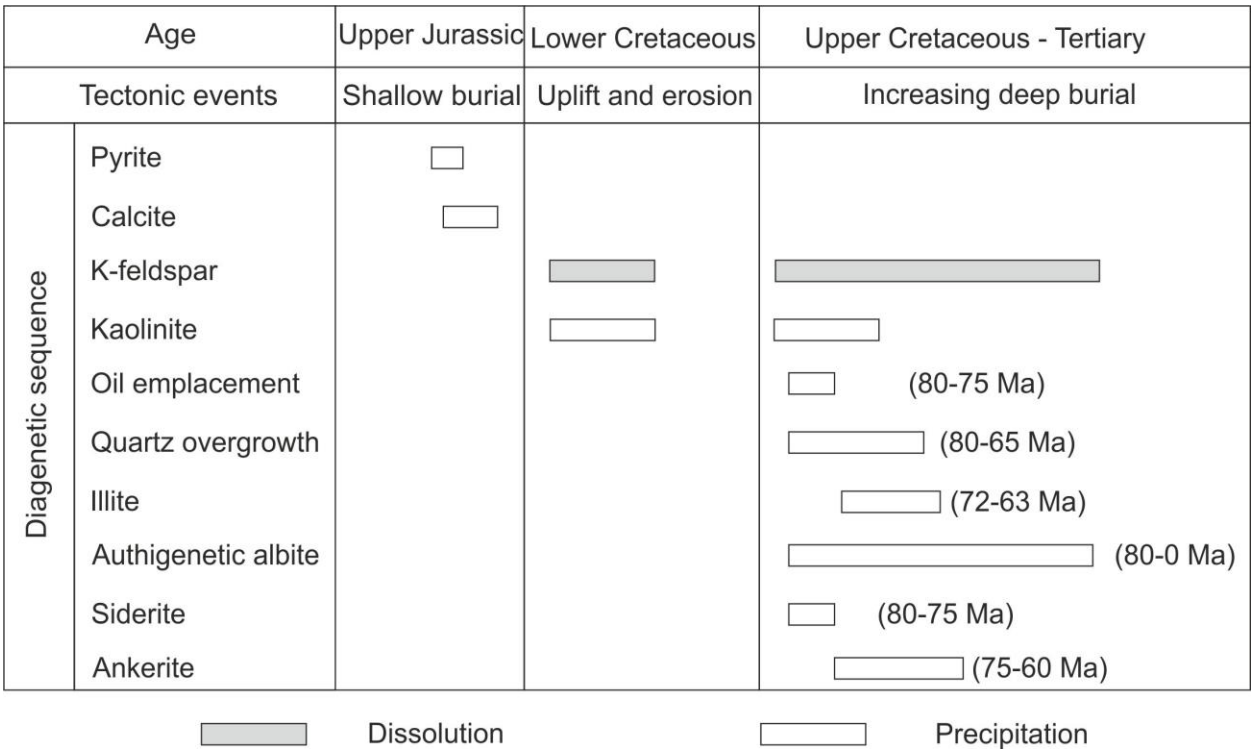
Age
Upper Jurassic
Lower Cretaceous
Upper Cretaceous - Tertiary
Tectonic events
Shallow burial
Uplift and erosion
Increasing deep burial
Diagenetic sequence
Pyrite
Calcite
K-feldspar
Kaolinite
Oil emplacement
(80-75 Ma)
Quartz overgrowth
(80-65 Ma)
Illite
(72-63 Ma)
Authigenetic albite
(80-0 Ma)
Siderite
(80-75 Ma)
Ankerite
(75-60 Ma)
Dissolution
Precipitation

Figure 7.

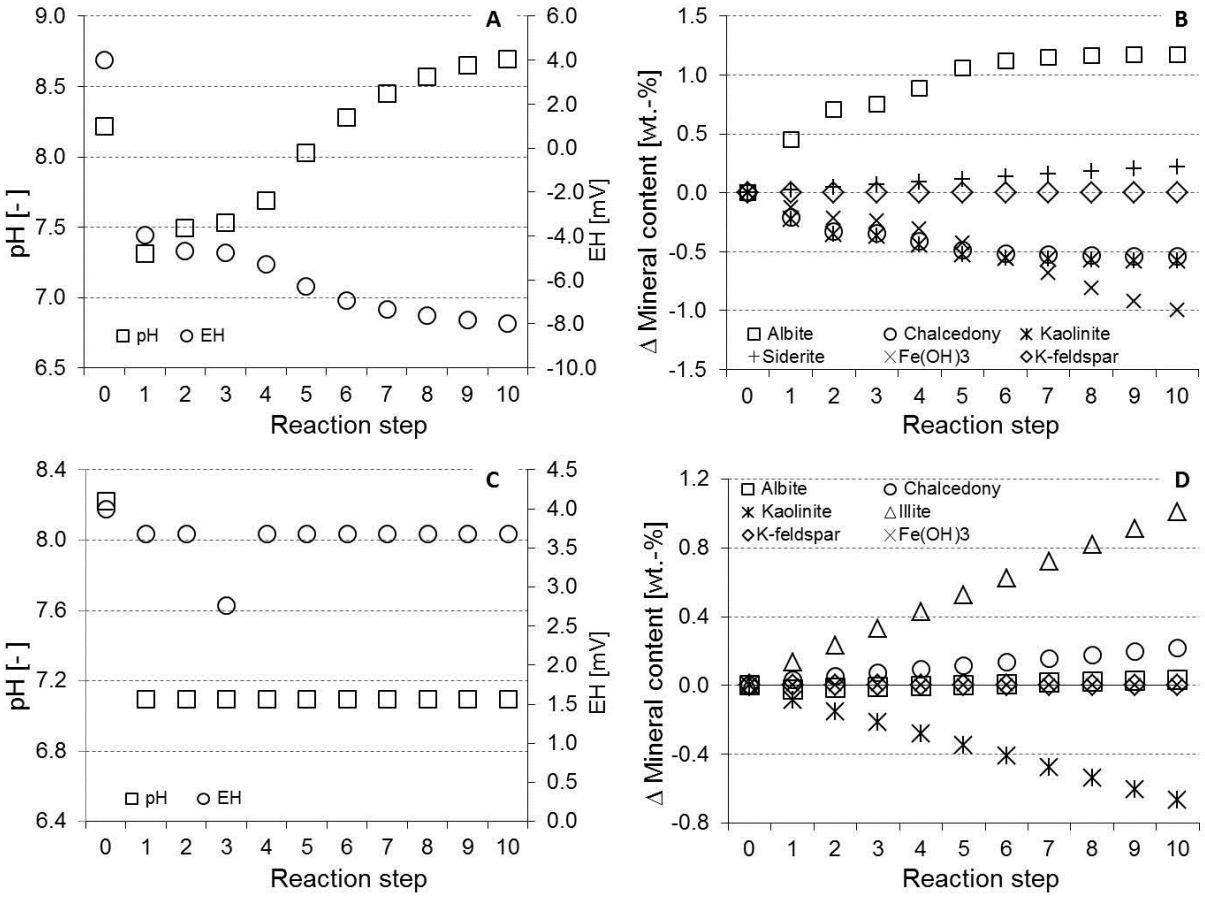
A
pH [-]
EH [mV]
pH
EH
Reaction step
B
Δ Mineral content [wt.-%]
Albite
Chalcedony
Kaolinite
Siderite
Fe(OH)3
K-feldspar
Reaction step
C
pH [-]
EH [mV]
pH
EH
Reaction step
D
Δ Mineral content [wt.-%]
Albite
Chalcedony
Kaolinite
Illite
Fe(OH)3
K-feldspar
Reaction step

Figure 8.

Table 1. Diagenetic features of the mineral assemblage in the Magnus oilfield[a].

	Detrital particles	Diagenetic features	
		Alteration	Formation
Quartz	x		overgrowth or fine crystals
K-feldspar	x[b]	x	
Albite	x[c]		overgrowth or replacive patch
Illite			fine filamentous crystals
Kaolinite			booklets
Siderite			rhombohedral crystal
Ankerite			cement
Pyrite			framboid

Blanks indicate that the corresponding features were not observed.

[a] Compare Fig. 2

[b] Including pure K-feldspar and perthite.

[c] Inherited from albitized K-feldspar from source areas cannot be excluded.

Table 2. Characteristics of feldspars in the Magnus field.

	Oligoclase	K-feldspar		Albite		
		unalbitized K-feldspar	K-feldspar reflicts	Albite overgrowth	Albite patch	Albite lamella
Habit	detrital grains	detrital grains	irregular patches	fresh euhedral crystals on detrital feldspar grains	irregular patches in albitized feldspar	Regular/irregular lamellae in perthite
Chemical composition	25% An	0-10% Ab and minor Ba	7% Ab and minor Ba	100% Ab	1-3% An	2-4% An
Texture	undissolved, with albite overgrowth	with/without albite lamellae	with micropores and pyrite	dense, without micropores or pyrite	with micropores, pyrite and/or mica inclusions	dense, without micropores and pyrite
Cathodoluminescence	yellow	bright blue	light yellow	dull	dull	dull
Origin	detrital	detrital	detrital	precipitation from formation water	replacement of K-feldspar	exsolution

An: anorthite.
Ab: albite.

Table 3. Present and pre-assigned mineral assemblages of the Magnus sandstones and reservoir conditions.

	Observed[a]		**Pre-assigned for modelling**		
	wt.-%	mol/kg		wt.-%	mol/kg
			Primary minerals[b]		
Quartz	65	114.68	Quartz	65	114.68
Albite	10	4.03	Albite[c]	8	3.22
K-feldspar	10	3.81	K-feldspar	12	4.57
Kaolinite	4	1.64	$Fe(OH)_3(a)$	1	0.99
Chalcedony[c]	2	3.53	Kaolinite	5	2.05
Ankerite	7	3.60	Chalcedony[d]	3	5.29
Siderite	1	0.91	**Secondary minerals**[e]		
Illite	1	0.27	Ankerite	0	0
			Siderite	0	0
			Illite	0	0
			Pyrite	0	0
Reservoir condition					
Temperature	116°C		116°C		
Pressure	450 atm		450 atm		

Notes:
[a] Based on petrographic observations and XRD analyses.
[b] Assumed original amounts of minerals before deep burial.
[c] Detrital albite is assumed.
[d] Primary quartz can only get dissolved; instead, chalcedony forms as secondary $SiO_{2(s)}$.
[e] Minerals allowed to precipitate in the generic modelling reactor.

1